EPR, FTIR, Optical absorption and photoluminescence studies of Fe_2O_3 and CeO_2 doped ZnO-Bi_2O_3-B_2O_3 glasses

Shiv Prakash Singh[a], R. P. S. Chakradhar[a], J. L. Rao[b], Basudeb Karmakar[a*]

[a] Glass Technology Laboratory, Glass Division,
Central Glass and Ceramic Research Institute (CSIR), Kolkata-700031, India
[b]Department of Physics, Sri Venkateswara University, Tirupati- 517 502, India.

Abstract

Glasses containing heavy metal oxide of the composition (wt %) $23B_2O_3$-$5ZnO$-$72Bi_2O_3$-xFe_2O_3/CeO2 ($0 \leq x \leq 0.0058$ atom % in excess) were prepared by melt quenching technique. The glass formation was confirmed by XRD. FTIR spectra exhibit characteristic absorption bands for B_2O_3 and Bi_2O_3 for their various structural units. The EPR spectra exhibit two resonance signals at $g \approx 6.4$ and $g \approx 4.2$ for Fe_2O_3 doped glasses. The resonance signals at $g \approx 4.2$ and $g \approx 6.4$ are attributed to Fe^{3+} ions in rhombic and axial symmetry sites respectively. The number of spins participating in resonance (N) and its paramagnetic susceptibility (χ) with composition has been evaluated. The effect of CeO_2 and Fe_2O_3 on optical and structural properties of zinc bismuth borate glass was investigated. From EPR and optical studies it is observed that iron ions are present in trivalent state with distorted octahedral symmetry. The cerium is present in Ce^{4+} state. Upon 400 nm excitation the emission at 548 nm and 652 nm are attributed to the Bi^{2+} species. The emission at 804 nm upon 530 nm excitation suggests that Bi^{+} ions are present in the sample. It is interesting to observe that the optical band gap energy (E_{opt}) decreases with the increase of transition metal and rare-earth ion doping.

Key words: Optical materials; Electron paramagnetic resonance; Optical spectroscopy; Luminescence

* Corresponding author. Tel.: +91 33 2473 3496; fax: +91 33 2473 0957.
E-mail address: basudebk@cgcri.res.in

1. Introduction

Glasses containing heavy metal oxide (HMO) have attracted attention of several researchers for excellent infrared transmission compared with the conventional glasses [1-3]. Attempts have been made to explore the mechanical, thermal and optical properties of these glasses. Among the other HMO glasses, bismuth oxide glasses have wide range of applications in the field of glass ceramics, layers for optical and electronic devices, thermal and mechanical sensors, reflecting windows [4-6]. Now-a-days lead oxide glasses have been restricted in various applications as it is hazardous to health and environment [7]. In this context, bismuth oxide has been a suitable substitution of lead oxide in glass preparation for its high refractive index, non-toxicity, wide transmission range, low melting temperature, etc. But the big problem associated with bismuth oxide glasses is its deep brown or black coloring as its concentration and melting temperature increases [8, 9]. Therefore, to obtain very high transmitting bismuth oxide glass is a technological challenge for the glass researchers. The properties of the glasses are closely related to inter-atomic forces and potentials in lattice structure. Thus any change in the lattice due to doping can be directly being noticed. The cerium dioxide and iron oxide can be used as a dopant in the bismuth glasses to remove its deep brown coloring as well as to improve its other optical, electrical and magnetic properties.

Glasses containing Fe_2O_3 are used in electrochemical, electronic and electro-optic devices [10-12]. The stability and semiconductor properties of Fe_2O_3 allow it to be used as a photocatalyst [13]. Despite numerous investigations, the semiconductor and optical properties of the iron oxides have been analyzed. The electronic structure of the iron oxides consists of Fe^{3+} ligand field transitions and excitations involving coupled adjacent

Fe^{3+} cations in the visible and near-UV range and ligand-to-metal charge-transfer transitions in the UV. The strong absorptivity of Fe_2O_3 in the visible range, along with its abundance and low cost, has stimulated considerable interest in its use as a photocatalyst and a photoelectrode. On the otherhand, glasses containing small amount of lanthanide ions have significant technological applications which use transitions between various electronic energy states. Many lanthanide ions have an incomplete 4f level which gives rise to the electronically forbidden f – f spectra in the ultraviolet, visible or infrared region. Cerium oxide is a rare earth oxide material from the lanthanide series. It is being used in various applications such as catalysts, fuel cells, solar cells, UV blocks, oxygen sensors, and polishing materials [14-16]. Cerium dioxide is extensively used due to its unique properties, in particular, high absorption capacity with respect to UV radiation and hardness and stability at high temperatures [17].

This study is focused on the synthesis of lead free high bismuth oxide containing ZnO-Bi_2O_3-B_2O_3 (ZBiB) glass system to which small quantity of CeO_2 and Fe_2O_3 were added as impurities in order to remove deep brown color formation and characterized them by using different spectroscopic techniques viz. FTIR, EPR, UV-Vis-NIR and photoluminescence (PL). We have systematically studied the EPR and optical absorption spectra of these glasses and interested to know the effect of impurities on spin-Hamiltonian parameters and also to know the site symmetry around Fe^{3+} ions in these glasses.

2. Experimental

The glass samples were prepared using bismuth trioxide, Bi_2O_3 (Loba Chemie), boric acid, H_3BO_3 (Loba Chemie), zinc oxide, ZnO (Loba Chemie), cerium dioxide, CeO_2 (Loba Chemie) and ferric oxide, Fe_2O_3 (Loba Chemie). The glass batch for 25 g glass of composition (wt %) $23B_2O_3$-5ZnO-$72Bi_2O_3$-$xCeO_2$

and $23B_2O_3$-5ZnO-$72Bi_2O_3$-yFe_2O_3 (x and y are excess in atom %) where, x = 0.0003, 0.0012, 0.003 and 0.0058, and y = 0.0003, 0.0012 and 0.003 was melted in a platinum crucible at 1150°C for 30 min with intermittent stirring for 0.5 min in an electrical furnace. The molten glass was cast onto a carbon plate and annealed at 420°C for 2h to release the internal stress. Samples of about 2 ± 0.01 mm thickness were prepared by cutting, grinding and polishing for optical measurements.

The X-ray diffraction studies was preformed with an X'pert Pro MPD diffractometer (PANalytical) operating at 45 kV and 35 mA using Ni-filtered CuKα (λ = 1.5406 *Å*) radiation and the X'celerator with step size 0.05º (2θ) and step time 0.5 sec from 10 to 80º. FTIR spectra were recorded by dispersing the glass powders in KBr with a Perkin-Elmer FTIR spectrometer (Spectrum 100). The UV-Vis absorption spectra in the range of 200-1100 nm were recorded using a double beam UV-visible spectrophotometer (Lambda 20, Perkin-Elmer). The fluorescence spectra were measured at an error of $\pm$0.2 nm with a fluorescence spectrophotometer (Fluorolog 2, Spex) using a 150 W Xe lamp as the excitation source and a photomultiplier tube (PMT) as detector. The excitation slit (1.25 mm) and emission slit (0.5 mm) were kept the same for luminescence measurements. The EPR spectra were recorded on a EPR spectrometer (JEOL-FE-1X) operating in the X-band frequency (≈ 9.200 GHz) with a field modulation frequency of 100 kHz. The magnetic field was scanned from 0 to 500 mT and the microwave power used was 5 mW. A powdered glass sample of 100 mg was taken in a quartz tube for EPR measurements.

3. Results and discussion

3.1. FTIR Studies

Fig. 1 shows the FTIR spectra for the (a) base glass ($23B_2O_3$-5ZnO-$72Bi_2O_3$, wt%), (b) 0.0058 Ce_2O_3 and (c) 0.003 Fe_2O_3 atom % doped glass at room temperature respectively. The FTIR spectra revealed characteristic absorption bands for B_2O_3 and Bi_2O_3 of their various structural units. The absorption band, observed at 678 cm^{-1}, is due to the bending vibration of B–O–B [18, 19] whereas the band at 924 cm^{-1} is due to asymmetric stretching vibration of the B–O bonds in BO_4 units and the broad band at

1330 cm^{-1} is attributed to the B–O bonds due to stretching vibration in the tetrahedral BO_3 units in the borate network [18-20]. The absorption bands at 448 cm^{-1} and 548 cm^{-1} are specific to the vibrations of Bi–O bonds in BiO_6 octahedral units [18, 20-21]. But the absorption band at 678 cm^{-1} has been assigned to symmetric stretching vibrations of Bi–O bonds in BiO_3 pyramidal units. This 678 cm^{-1} absorption band can also be assigned to B–O–B bending vibrations [18, 20], which could be superposed with the stretching vibrations of Bi–O bonds in BiO_3 pyramidal units. With the addition of 0.0058 atom % of CeO_2 and 0.003 atom % of Fe_2O_3 to the glass system, the absorption bands at 448 and 548 cm^{-1} for Bi–O bonds in BiO_6 octahedral units became weak. This observation indicates the structural changes occurred between Bi–O bonds, Ce–O and Fe–O bonds. Cakić et al. [22] reported the absorption bands for Fe–O in octahedral structural units of FeOOH at 465 cm^{-1}. It must be noted that the bands corresponding to the FTIR absorption of Fe–O and Ce–O were not directly evidenced in the glass matrix, but the bands at 448 cm^{-1} and 548 cm^{-1} assigned to Bi–O in BiO_6 octahedral unit become weaken by the addition of 0.0058 atom % of CeO_2 and 0.003 atom % of Fe_2O_3 for their characteristic absorption bands.

3.2. EPR Studies

The EPR spectra of the undoped glasses have not shown any absorption indicating that the base glass is pure from paramagnetic impurities and defects. But the glass doped with the Fe_2O_3 shows resonance signal, which are characteristic of Fe^{3+} ions in distorted octahedral symmetry sites. Fig. 2 shows typical EPR spectrum for Fe^{3+} ions in $23B_2O_3$-$5ZnO$-$72Bi_2O_3$-xFe_2O_3 (x = 0.0003, 0.0012 and 0.003 atom %) glasses at room temperature. The EPR spectra mainly consists of an intense resonance signal at $g \approx 4.2 \pm$

0.1 when Fe_2O_3 content is ≤ 0.0012 atom %. When Fe_2O_3 content is 0.003 atom % the EPR spectrum shows in addition to g ≈ 4.2 ± 0.1 signal a shoulder in the region of g ≈ 6.4 ± 0.1. As the iron ions are in Fe^{3+} state belongs to d^5 configuration with ^6S as ground state in the free ion and there is no spin-orbit interaction [23]. The g value is expected to lie very near the free-ion value. However a g value very much greater than 2.0 often occurs; in particular an isotropic g value at 4.2 occurs and these large g values arise when certain symmetry elements are present. The theory of these large g values is usually expressed by the spin-Hamiltonian [24]

$$H = g\beta BS + D [S_Z^2 - \{ S (S+1) / 3\}] + E (S_x^2 - S_y^2) \qquad (1)$$

where S = 5/2. Here D and E are the axial and rhombic structure parameters, λ = E/D lies within the limits $0 < \lambda < 1/3$ [25]. The isotropic resonance at g = 4.2 corresponds to λ = 1/3. This feature at g = 4.2 is due to rhombic distortions of the crystal field around Fe^{3+} ions [26, 27]. In a large number of glasses and with Fe^{3+} containing materials a symmetric and isotropic line at g ≈ 4.0 - 4.2 is observed. Castner et al. [28] explained it as arising from the middle Kramers doublet containing admixture of different $|\pm m_j>$ states, which are caused by the presence of low symmetry term E $(S_x^2 - S_y^2)$ in the spin-Hamiltonian.

The EPR spectra of Fe^{3+} ions in glasses are generally characterized by the appearance of resonance signals at g = 2.0, g = 4.2 and g = 6.0 with their relative intensities being strongly dependent on composition [29-39]. Usually, the occurrence of two resonance signals, at g ≈ 4.2 and g ≈ 2.0 has been reported [28]. In some cases, a resonance near g ≈ 6.0 was also observed [28, 40] as a shoulder of the resonance near g ≈

4.2. The g = 2.0 resonance is assigned to those ions which interact by exchange coupling and can be considered as distributed in clusters [36-39].

The resonance signals at g ≈ 4.2 and g ≈ 2.0 were discussed by many investigators [29-31]. Some investigators [28, 41] suggested that the value of g in glasses containing Fe^{3+} ions is related to the coordination number. The absorption at g ≈ 4.2 and g ≈ 2.0 arise from Fe^{3+} ions in tetrahedral and octahedral coordinations respectively [30]. Kurkjian and Sigety [29] showed that the resonance signals at g ≈ 4.2 and g ≈ 2.0 cannot be used as a direct indication of coordination number for Fe^{3+} ions and suggested that the g ≈ 4.2 resonance signal is due to low symmetry (rhombic) sites of either tetrahedral or octahedral coordination. This interpretation has been supported by Loveridge and Parke [23]. An effective g value of g_{eff} ≈ 9.7 was also reported for Fe^{3+} ions in glasses [32, 33]. According to Wickman et al. [42], Fe^{3+} ions in rhombic vicinities show the transition having g ≈ 4.2 isotropic value corresponding to middle Kramers doublet.

In the present study, the EPR spectra mainly consists of an intense resonance signals at g ≈ 4.2 and a shoulder in the region of g ≈ 6.4. The resonances at g ≈ 4.2 is attributed to the isolated Fe^{3+} ions predominantly situated in rhombically distorted octahedral sties where as g ≈ 6.4 resonance arise from axially distorted sites respectively. In the present study we did not observe the g = 2.0 resonance indicating that iron ions are free from clusters there by there is no exchange coupling interactions between them. Since the authors doped very low quantity of iron, and therefore this also supports our above conclusion (free from cluster). It is interesting to note further that, g ≈ 6.4 resonance is observed only for 0.003 Fe_2O_3 indicating that iron ions are free from axially distorted sites if the doping is less than 0.0058 atom%. From the observed g values, it is clear that

the iron ions are in trivalent state and the site symmetry is distorted octahedral in these glasses.

3.3. Spins (N) participating in resonance

The number of spins participating in a resonance can be calculated by comparing the area under the absorption curve with that of a standard ($CuSO_4.5H_2O$ in this study) of known concentration. Weil et al. [43] gave the following expression which includes the experimental parameters of both sample and standard.

$$N = \frac{A_x\,(Scan_x)^2\,G_{std}\;(B_m)_{std}\;(g_{std})^2\,[S\,(S+1)]_{std}\,(P_{std})^{1/2}}{A_{std}\,(Scan_{std})^2\;G_x\,(B_m)_x\,(g_x)^2\;[S\,(S+1)]_x\;(P_x)^{1/2}}\;[Std] \qquad (2)$$

where A is the area under the absorption curve which can be obtained by double integrating the first derivative EPR absorption curve, *scan* is the magnetic field corresponding to unit length of the chart, G is the gain, B_m is the modulation field width, g is the g factor**,** S is the spin of the system in its ground state. P is the power of the microwave. The subscripts '*x*' and '*std*' represent the corresponding quantities for Fe^{3+} glass sample and the reference ($CuSO_4.5H_2O$) respectively. The number of spins participating in resonance at $g \approx 4.2$ has been calculated as a function of iron content by using the above equation (2). It is observed that N varies from 0.15×10^{21}, 0.24×10^{21} and 2.35×10^{21} spins/kg for 0.0003, 0.0012 and 0.003 atom % of Fe_2O_3 respectively. The EPR data is used to calculate the paramagnetic susceptibility (χ) at room temperature by using the formula [44]

$$\chi = \frac{N g^2 \beta^2 J(J+1)}{3k_B T} \qquad (3)$$

where N is the number of spins per m^3 and the other symbols have their usual meaning . N can be calculated from equation (2) and $g \approx 4.2$ is taken from EPR data. The paramagnetic susceptibility (χ) evaluated from EPR data varies from 0.165×10^{-3}, 0.258×10^{-3} and 2.526×10^{-3} m^3/kg for 0.0003, 0.0012 and 0.003 atom % of Fe_2O_3 respectively. We chose to determine the spin susceptibility from EPR spectra, because in this technique, the main advantage is the diamagnetic contribution must be subtracted off, which is not possible in a static measurement.

3.4. UV-Vis-NIR absorption studies

The color of the as prepared glass changes gradually as CeO_2 and Fe_2O_3 concentrations added in these glasses. The as prepared base glass appeared in deep black color, but it becomes yellow to light yellow and again deep yellow after addition of 0.0003, 0.0012, 0.003 and 0.0058 atom % of CeO_2 and 0.0003, 0.0012 and 0.003 atom % of Fe_2O_3. The measured UV–Vis optical spectra of the undoped as well as 0.0003, 0.0012, 0.003 and 0.0058 atom % of CeO_2 and 0.0003, 0.0012 and 0.003 atom % of Fe_2O_3 doped in $23B_2O_3$-5ZnO-$72Bi_2O_3$ (wt. %) glasses reveal spectral changes as discussed below.

The undoped $23B_2O_3$-5ZnO-$72Bi_2O_3$ (wt. %) glass system did not show any absorption peaks from 400–1100 nm (Figs. 3 and 4). The CeO_2 and Fe_2O_3 addition have shown the distinct absorption bands at higher concentrations. In CeO_2 doped glasses show absorption band at 411 and 431 nm for 0.003 and 0.0058 atom % concentrations

respectively (Fig. 3). On the other hand, Fe_2O_3 doped glasses exhibit distinct absorption bands at 408 and 424 nm for 0.0012 and 0.003 atom % concentrations respectively (Fig. 4). In both the cases the absorption bands are shifting towards the higher wavelength side with increase in doping concentration. It is known that for Fe^{3+} ions, there are no spin-allowed transitions and the bands observed are due to spin-forbidden transitions only. In the present study weak absorption bands observed at 408 and 424 nm for 0.0012 and 0.003 atom % concentrations of Fe_2O_3 have been assigned to the transitions $^6A_{1g}(S) \rightarrow {}^4A_{1g}(G)$, $^4E_g(G)$. The observed band positions are compared with those found in many glass systems containing iron, which indicates that iron ions are present in trivalent state with distorted octahedral symmetry [45-47].

For CeO_2 doped glasses the observed absorption bands at 411 and 431 nm for 0.003 and 0.0058 atom % CeO_2 (Fig. 3) can be attributed to an excitonic absorption peak. Hirani and Hogarth [48] gave a similar interpretation for their optical studies in phosphate glasses. Tashiro et al. [49] observed optical absorption bands for Ce^{3+} at 294, 245 and 227 nm in phosphate glasses. The absence of these peaks in our studies suggests that in the present study cerium is believed to be in Ce^{4+} state which has no characteristic absorption bands in this region [50]. Further, our photoluminescence studies did not reveal any luminescence spectrum for Ce^{3+} in glasses which also supports that in the present work glasses do not contain Ce^{3+}, hence the cerium in the present system exist in Ce^{4+} state.

The optical absorption near the edge is strongly dependent on the electronic structure, and in amorphous or glassy materials, the band tail arising from the randomness of the bonding gives rise to some difficulties of interpretation. The

absorption processes are depending on the nature of transitions, either direct or indirect, or forbidden or permitted, the index n in the equation for optical absorption coefficient may be estimated, particularly at the higher values of α (υ), by fitting to the experimental results as given by the relation.

$$\alpha(\upsilon) = B(h\upsilon - E_{opt})^n / h\upsilon \quad (4)$$

where, B is a constant, hυ is the photon energy and E_{opt} is the optical energy gap.

A reasonable fit of equation (4) with n = 2 is achieved for many amorphous non-metallic materials and suggests absorption by indirect transitions. Figs. 5 and 6 show the variation of optical band gap energy as a function of concentration of CeO_2 and Fe_2O_3 respectively.

In the present study, with doping the shift of the absorption peaks to longer wavelength results in the gradual decrease in the optical band gap which are shown in Figs. 5 and 6. A recent study by Saritha et al. [51] in the $ZnO\text{-}Bi_2O_3\text{-}B_2O_3$ glass system has shown that the value of E_{opt} decreases in the range 3.464 - 3.169eV with increase in Bi_2O_3 concentration from 25 to 50 mol%. The shift is attributed to the structural changes which are the result of the different site occupations.

3.5. Photoluminescence Studies

The photoluminescence measurement was carried out for undoped, CeO_2 (0.0003, 0.0012, 0.003 and 0.0058 atom %) and Fe_2O_3 (0.0003, 0.0012 and 0.003 atom %) doped bismuth glasses. The emission bands at 548 nm and 652 nm were recorded when excited at 400 nm are shown in Figs. 7 and 8. The intensity of the peaks at 548 and 652 nm for the CeO_2 doped glass increases up to concentration of 0.0012 atom % and decreases at higher concentrations (0.003 and 0.0058 atom %). However, in case of Fe_2O_3, the

intensity decreases with the increase in the concentration. The other emission band observed at 804 nm when excited at 530 nm for CeO_2 and Fe_2O_3 doped are shown in Figs. 9 and 10 respectively. The intensity of the 804 nm peak increase in CeO_2 concentration. In case of Fe_2O_3 doped glass the intensity of the peak at 804 nm, initially increases for $Fe_2O_3 \leq 0.0012$ atom % and then after decreases at the concentration of 0.003 atom %.

Luminescent properties of Bi^{3+} in glasses have been investigated by various researchers [2, 52-54]. The ground state of the Bi^{3+} ion is $^1S_0$, whereas the 6s6p excited states give rise to $^3P_0$, $^3P_1$, $^3P_2$ and $^1P_1$ in the order of increasing energy. Because the $^1S_0 \rightarrow {}^3P_0$ and $^1S_0 \rightarrow {}^3P_2$ transitions are strongly forbidden, the Bi^{3+} transitions between the $^1S_0$ ground state and the $^3P_1$ or $^1P_1$ excited state are usually observed. The different researchers [2, 54] have proposed the excitation of Bi^{3+} ion appear in the ultraviolet region, while the emission peak of Bi^{3+} ion is not located in one characteristic spectral region but varies from the ultraviolet region into the red region with differing host lattice. Therefore, in this study, the emission bands are recorded in visible to infrared region when excited in the visible region. Hence, these emission bands are not due to Bi^{3+} ion. On the other hand the Bi^{2+} ion has $6s^26p^1$ configuration, and thus one has to consider a single p electron. The ground state configuration $6s^26p^1$ is split by spin orbit coupling interaction into $^2P_{1/2}$ ground state and $^2P_{3/2}$ in the order of increasing energy. In the energy diagram proposed by Zhou et al. [54], the $^2P_{3/2}$ is further split into two crystal field terms, which are denoted as $^2P_{3/2}$ (1) and $^2P_{3/2}$ (2) in the order of increasing energy. From the energy diagram, the excitation at wavelength 400 nm can be ascribed to $^2P_{1/2} \rightarrow {}^2P_{3/2}$ (2) transition. The emission bands centered at 548 is due to the $^2P_{3/2}$ (1) $\rightarrow {}^2P_{1/2}$ transition. Hamstra et al [55] have found red emission band at 625 nm for Bi^{2+} ion. So the observed

emission band at 652 nm can be attributed to Bi^{2+} ion. In case of Bi^{+} ion, energy level study is difficult because of the presence of two 6p electrons in the ground state configuration. The analysis is based on the calculated model for the $6s^26p^2$ configuration. The mutual electrostatic interaction of two 6p electrons splits the ground state configuration into three terms: ^3P, ^1D, and ^1S, in the order of increasing energy. Spin-orbit interaction further splits the ground term into fine structure levels: $^3P_0$, $^3P_1$ and $^3P_2$, in ascending order. According to energy diagrams proposed by Meng et al. [2] and Zhou et al. [54] the excitation band at 530 nm corresponds to the $^3P_0 \rightarrow {}^1S_0$ transition. A band in the infrared region at 804 nm resulting from the $^3P_2 \rightarrow {}^3P_0$ transition is due to lower valence of bismuth ion (Bi^{+}). The extended nature of 6p orbital in Bi^{+} ion also plays an important role in the luminescent properties due to the crystal field effect. The emission band in the infrared region due to Bi^{+} ion has also suggested by Sun et al. [56] and Qiu et al. [57]. Thus, the excitation wavelength dependent infrared luminescence may be attributed to site-to-site variations in the environment of the emission centers.

The intensity of observed emission bands at 548 and 652 nm in case of CeO_2 doped glasses show the increasing order up to concentration of 0.0012 atom % and then further decreases. This phenomenon happens probably due to quenching effect at this threshold concentration. This observation also established by the absorption bands at 411 and 431 nm of higher concentrations of CeO_2. Therefore, at higher concentration the intensity of the emission band decreases as the excitation energy of Bi^{2+} and absorption band of Ce^{4+} are nearly the same. So the excitation energy of Bi^{2+} is absorbed by Ce^{4+} which results in the decrease of intensity. The same fact has also observed in case of Fe_2O_3 doped samples as its absorption band due to Fe^{3+} ion and excitation energy of Bi^{2+}

ion are in similar range of energy. But the intensity of emission due to Bi^{+} ion in CeO_2 doped glasses are increasing order may be due to energy transfer from the Ce^{4+} energy level to the Bi^{+} energy levels. In the case of Fe_2O_3 doped glasses the same phenomenon happened may be due to the same reason. But at higher concentration (0.003 atom %) the intensity decreases due to the effect of energy quenching.

4. Conclusions

Zinc-bismuth-borate glasses with iron and cerium doping have been prepared by melt quenching technique. The as prepared base glass appeared in deep brown color, but it becomes yellow to light yellow and again deep yellow after addition of 0.0003, 0.0012, 0.003 and 0.0058 atom % of CeO_2 and 0.0003, 0.0012 and 0.003 atom % of Fe_2O_3. The FTIR spectra reveal 678 cm^{-1}, is due to the bending vibration of B–O–B in BO_3 trigonal unit. The band at 924 cm^{-1} is due to asymmetric stretching vibration of the B–O bonds in BO_4 units and the broad band at 1330 cm^{-1} is attributed to the B–O bonds due to stretching vibration in the trigonal BO_3 units in the borate network. The other absorption bands at 448 cm^{-1} and 548 cm^{-1}, specific to the vibrations of Bi–O bonds in BiO_6 octahedral units. The EPR spectra of Fe^{3+} ions exhibit two resonance signals at $g \approx 4.2$ and $g \approx 6.4$ which are attributed to Fe^{3+} ions in rhombic and axial symmetry sites respectively. The absorption bands observed at 408 and 424 nm for 0.0012 and 0.003 atom % concentrations of Fe_2O_3 have been assigned to the transitions $^6A_{1g}(S) \rightarrow {}^4A_{1g}(G)$, $^4E_g(G)$. From EPR and optical studies it is observed that iron ions are present in trivalent state with distorted octahedral symmetry. For CeO_2 doped glasses the observed absorption bands at 411 and 431 nm for 0.003 and 0.0058 atom % CeO_2 can be attributed

to an excitonic absorption peaks. The cerium is present in Ce^{4+} state. The emission at 548 nm and 652 nm are attributed to the Bi^{2+} species when excited at 400 nm. The emission band at 804 nm is due to Bi^{+} ions when excited at 530 nm. The optical bandgap (E_{opt}) decreases with increase of transition metal and rear earth dopants.

Acknowledgements

The authors gratefully acknowledge the financial support of NMITLI, CSIR, New Delhi. They gratefully thank Dr. H. S. Maiti, Director of the institute for his keen interest and kind permission to publish this paper. The technical support provided by the Bioceramics Division of this institute for recording FTIR spectra is also thankfully acknowledged.

References

[1] Y. Fujimoto, M. Nakatsuka, Jpn. J Appl. Phys. 40 (2001) L279.

[2] X. Meng, J. Qiu, M. Peng, D. Chen, Q. Zhao, X. Jiang, C. Zhu, Opt. Express 13 (2005) 1635.

[3] B. Denker, B. Galagan, V. Osiko, S. Sverchkov, E. Dianov, Appl. Phys. B 87 (2007) 135.

[4] I. Opera, H. Hesse, K. Betzler, Opt. Mater. 26 (2004) 235.

[5] X. Zhao, X. Wang, H. Lin, Z. Wang, Physica B 390 (2007) 293.

[6] M. Łaczka, L. Stoch, J. Górecki, J. Alloys Compd. 186 (1992) 279.

[7] J. An, J-S. Park, J-R Kim, K. S. Hong, H. Shin, J. Am. Ceram. Soc. 89 (2006) 3658.

[8] O. Sanz, E. Haro-Poniatowski, J. Gonzalo, J. M. Fernández Navarro. J. Non-Cryst. Solids 352 (2006) 761.

[9] Y. Zhang, Y. Yang, J. Zheng, W. Hua, G. Chen, J. Am. Ceram. Soc. 91 (2008) 3410.

[10] U. Selvaraj, K. J. Rao, J. Non-Cryst. Solids 72 (1985) 315.

[11] N. Satyanarayana, G. Govindaraj, A. Karthikeyan, J. Non-Cryst. Solids 136 (1991) 219.

[12] M. Jamnicky, P.Znasic, D. Tunega, M. D. Ingram, J. Non-Cryst. Solids 185 (1995) 151.

[13] N. J. Cherepy, D. B. Liston, J. A. Lovejoy, H. Deng, and J. Z. Zhang, J. Phys. Chem. B 102 (1998) 770.

[14] X. D. Feng, D. C. Sayle, Z. L. Wang, M. S. Paras, B. Santora, A. C. Sutorik, , T. X. T. Sayle, Y. Yang, Y. Ding, , X. D. Wang, Y. S. Her, Science 312 (2006) 1504.

[15] R. Si, Y. W. Zhang, S. J. Li, B. X. Lin, C. H. Yan, J. Phys. Chem. B 108 (2004) 12481.

[16]. K. B. Zhou, Z. Q. Yang, S. Yang, Chem. Mater. 19 (2007) 1215.

[17] A. Trovarelli, , C. de Leitenburg, , M. Boaro, G. Dolcetti, , Catal. Today, 50 (1999) 353.

[18] A. H. Doweidar, Y. B. Saddeek, J. Non-Cryst. Solids 355 (2009) 348.

[19] B. S. G. Motke, S. P. Yowale and S. S. Yawale, Bull. Mater. Sci. 25 (2002) 75.

[20] C. Y. B. Saddeek, M. S. Gaafar, Mater. Chem. Phys. 115 (2009) 280.

[21] M. Bosca, L. Pop, G. Borodi, P. Pascuta, E. Culea, J. Alloys Compd. 479 (2009) 579.

[22] D. M. D. Cakić, G. S. Nikolić, L. A. Ilić, Bull. Chem. Technol. Macedonia, 21 (2002) 135.

[23] D. Loveridge , S. Parke, Phys. Chem. Glasses 12 (1971) 90.

[24] B. Bleaney, K. W. H. Stevens Rep. Prog. Phys. 16 (1953) 108.

[25] J. H. Van Vleck, W. G. Penny, Phil. Mag. 17 (1934) 961.

[26] A. Abragam, B. Bleaney, Electron Paramagnetic Resonance of Transition Ions, Oxford, Clarendon 1970.

[27] R. K. Singh, G. P. Kothiyal, A. Srinivasan, J. Non-Cryst. Solids, 354 (2008) 3166.

[28] T. Castner, G. S. Newell Jr., W. C. Holton, C. P. Slichter J. Chem. Phys., 32 (1960) 668.

[29] C. R. Kurkjian, E. A. Sigety, Phys. Chem. Glasses 9 (1968) 73.

[30] C. Hirayama, J. G. Castle Jr., M. Kuriyama Phys. Chem. Glasses, 9 (1968) 109.

[31] J. S. Griffith, Mol. Phys. 8 (1964) 213.

[32] C. Legin, J. Y. Buzare, C. Jacoboni J. Non-Cryst. Solids, 161 (1993) 112.

[33] I. Ardelean, M. Peteanu, S. Flip, V. Simon, G. D. Gyorffy, Solid State Commun. 102 (1997) 341.

[34] F. Y. Olivier, B. Boizot, D. Ghaleb, G. D. Petite J. Non-Cryst. Solids 351 (2005) 1061.

[35] C. Horea, D. Rusu, I. Ardelean, J Mater Sci: Mater Electron 20 (2009) 905.

[36] D. W. Moon, J. M. Aitken, R. K. MacCrone, G. S. Cieloszzyk, Phys. Chem. Glasses, 16 (1975) 91.

[37] E. Burzo, I. Ardelean, Phys. Status Solidi B, 87 (1978) K137.

[38] T. Komatsu, N. Soga, J. Chem. Phys. 73 (3) (1980) 1781.

[39] M. Nofz, R. Stosser, F. G. Wihsmann, Phys. Chem. Glasses, 31 (1990) 57.

[40] E. M. Yahiaoui, R. Berger, T. Servant, J. Kliava, L. Cugunov, A. Mednir, J. Phys.: Condens. Mater., 6 (1994) 9415.

[41] J. R. Pilbrow, Transition Ion Electron Paramagnetic Resonance, Oxford, Clarendon, p.135 1990.

[42] H. H. Wickman, M. P. Klein, D. A. Shirley, J. Chem. Phys. 42 (1965) 2113.

[43] J. A. Weil, J. R. Bolton, J. E. Wertz, Electron Paramagnetic Resonance – Elementary Theory and Practical Applications Wiely, New York, p. 498, 1994.

[44] N. W. Aschcroft and N. D. Mermin. "Solid State Physics" Harcourt College Publishers, (2001) p.656.

[45] T. Bates, in: J.D. Mackenzie (Ed.) Modern Aspects of the Vitreous State, vol. 2. Butterworths, London, p. 242,1962..

[46] T. Abrita, F. S. Barrros, J. Lumin. 40 (1988) 187.

[47] M. L. Baesso, E. C. da Silva, F. C. G. Gandra, H. Vargas, P.P. de Areu Filho, F. Galembeck, Phys. Chem. Glasses. 31 (1990) 123.

[48] R. Hirani, C. A. Hogarth, J. Mater. Sci. Lett., 8 (1989) 150.

[49] M. Tashiro, N. Soga, S. Sakka, J**.** Ceram**.** Ass**.** Japan, 68 (1960) 132.

[50] A. M. Bishay, J. Am. Ceram. Soc. 45 (1962) 8.

[51] D. Saritha, Y. Markandeya, M. Salagram, M. Vithal, A. K. Singh and G. Bhikshamaiah, J. Non-Cryst. Solids. 354 (2008) 5573.

[52] G. Blasse, A. Brill, J. Chem. Phys. 47 (1967) 1920.

[53] G. Blasse, A. Brill, J. Chem. Phys. 48 (1968) 217.

[54] S. Zhou, N. Jiang, B. Zhu, H. Yang, S. Ye, G. Laksminarayana, J. Hao, J. Qiu, Adv. Funct. Mater. 18 (2008) 1407.

[55] M. A. Hamstra, H. F. Folkerts, G. Blasse, J. Mater. Chem. 4 (1994) 1349.

[56] H. T Sun, A. Hosokawa, Y. Miwa, F. Shimaoka, M. Fujii, M. Mizuhata, S. Hayashi, S. Deki, Adv. Mater. 21 (2009) 1.

[57] J. Qiu, M. Peng, J. Ren, X. Meng, X. Jiang, C. Zhu, J. Non-Cryst. Solids 354 (2008) 1235.

Figure captions

Fig. 1. FTIR spectra of the (a) base glass, (b) 0.0058 atom % CeO_2 and (c) 0.003 atom % Fe_2O_3 doped $23B_2O_3$-5ZnO-$72Bi_2O_3$ glasses.

Fig. 2. EPR spectra of the Fe^{3+} ions in (a) 0.0003, (b) 0.0012 and (c) 0.003 atom % Fe_2O_3 doped $23B_2O_3$-5ZnO-$72Bi_2O_3$ glasses.

Fig. 3. Optical absorption spectra of (a) 0 (base glass) and (b) 0.0003, (c) 0.0012, (d) 0.003 and (e) 0.0058 atom % CeO_2 doped $23B_2O_3$-5ZnO-$72Bi_2O_3$ glasses.

Fig. 4. Optical absorption spectra of (a) base glass (b) 0.0003 (c) 0.0012 and (d) 0.003 atom % Fe_2O_3 doped $23B_2O_3$-5ZnO-$72Bi_2O_3$ glasses.

Fig. 5. Variation of optical bandgap energy with CeO_2 content in $23B_2O_3$-5ZnO-$72Bi_2O_3$-x(CeO_2 in excess) glass.

Fig. 6. Variation of optical bandgap energy with Fe_2O_3content in $23B_2O_3$-5ZnO-$72Bi_2O_3$-x(Fe_2O_3 in excess) glass.

Fig. 7. Photoluminescence spectra of (a) 0 (base glass), (b) 0.0003, (c) 0.0012, (d) 0.003 and (e) 0.0058 atom % CeO_2 doped $23B_2O_3$-5ZnO-$72Bi_2O_3$ glasses at $\lambda_{ex.}$ = 400 nm.

Fig. 8. Photoluminescence spectra of (a) 0 (base glass), (b) 0.0003 (c) 0.0012 and (d) 0.003 atom % Fe_2O_3 doped $23B_2O_3$-5ZnO-$72Bi_2O_3$ glasses at $\lambda_{ex.}$ = 400 nm.

Fig. 9. Photoluminescence spectra of (a) 0 (base glass), (b) 0.0003, (c) 0.0012, (d) 0.003 and (e) 0.0058 atom % CeO_2 doped $23B_2O_3$-5ZnO-$72Bi_2O_3$ glasses at $\lambda_{ex.}$ = 530 nm.

Fig. 10. Photoluminescence spectra of (a) 0 (base glass), (b) 0.0003 (c) 0.0012 and (d) 0.003 atom % Fe_2O_3 doped $23B_2O_3$-5ZnO-$72Bi_2O_3$ glasses at $\lambda_{ex.}$ = 530 nm.

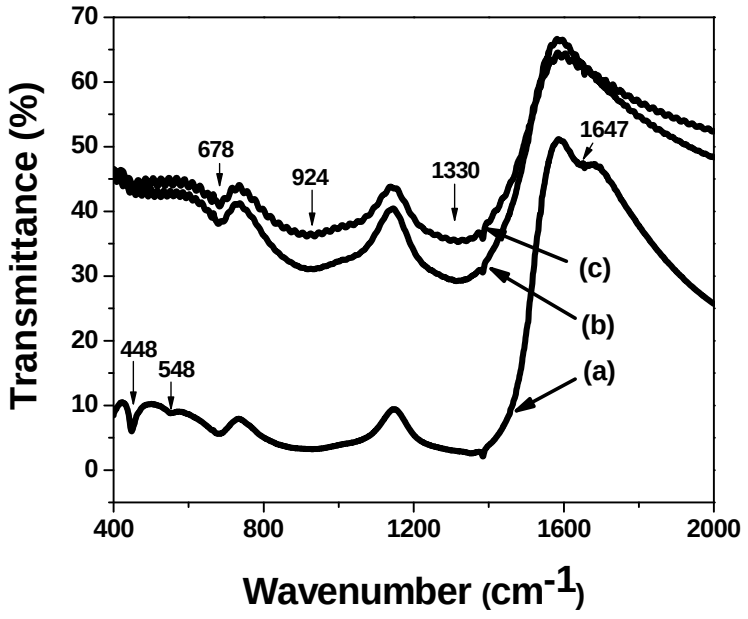

Fig. 1. FTIR spectra of the (a) base glass, (b) 0.0058 atom % CeO_2 and (c) 0.003 atom % Fe_2O_3 doped $23B_2O_3$-5ZnO-$72Bi_2O_3$ glasses.

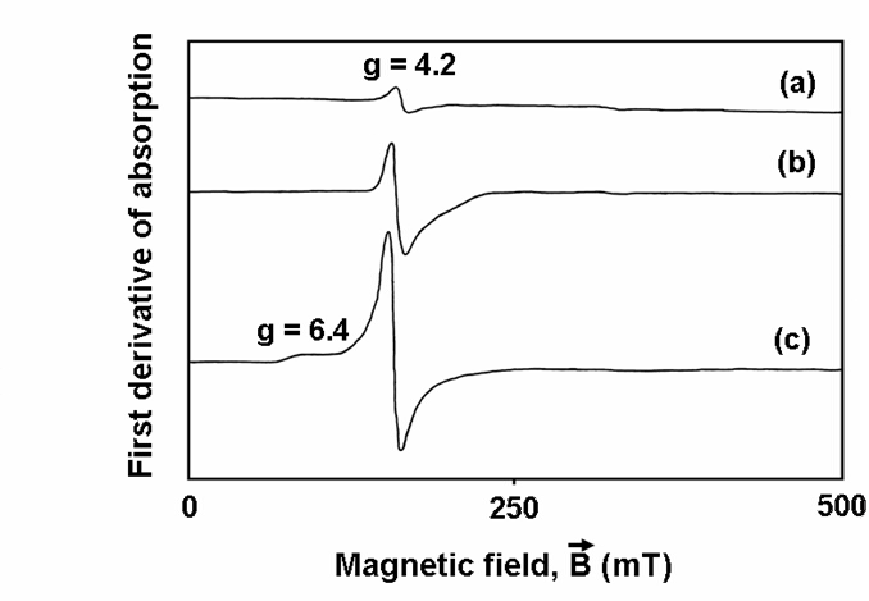

Fig. 2. EPR spectra of the Fe^{3+} ions in (a) 0.0003, (b) 0.0012 and (c) 0.003 atom % Fe_2O_3 doped $23B_2O_3$-5ZnO-$72Bi_2O_3$ glasses.

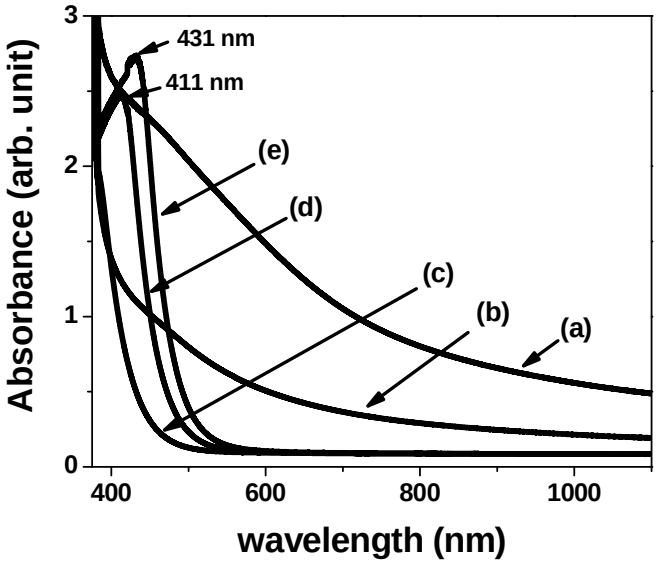

Fig. 3. Optical absorption spectra of (a) 0 (base glass) and (b) 0.0003, (c) 0.0012, (d) 0.003 and (e) 0.0058 atom % CeO_2 doped $23B_2O_3$-5ZnO-$72Bi_2O_3$ glasses.

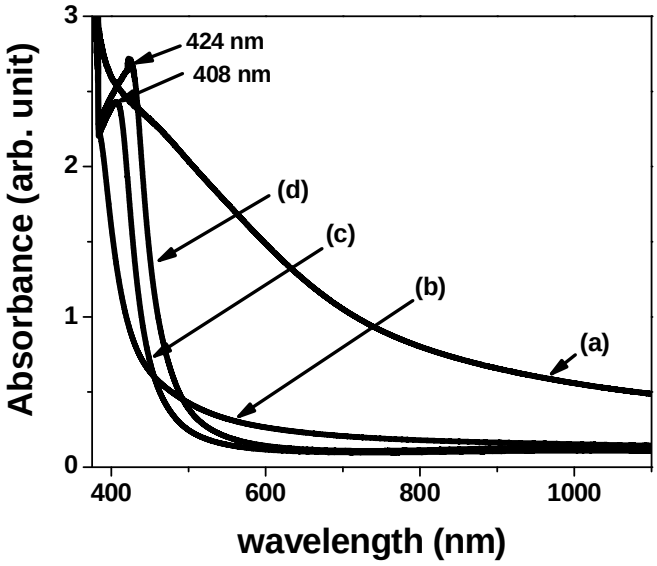

Fig. 4. Optical absorption spectra of (a) base glass (b) 0.0003 (c) 0.0012 and (d) 0.003 atom % Fe_2O_3 doped $23B_2O_3$-5ZnO-$72Bi_2O_3$ glasses.

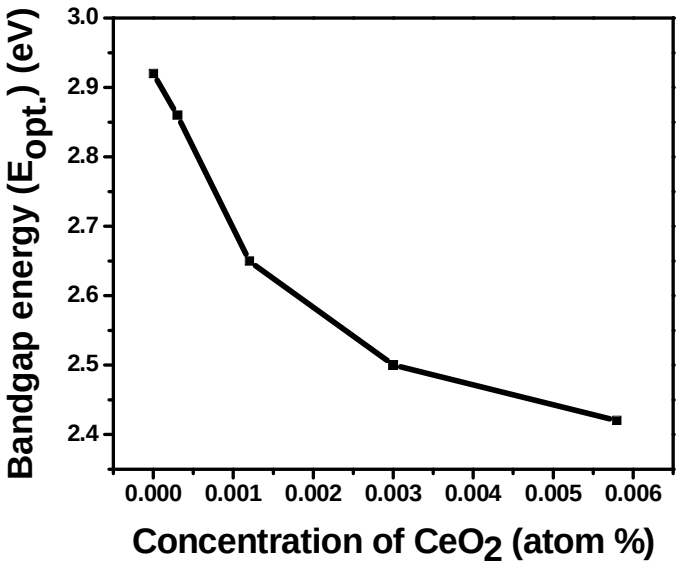

Fig. 5. Variation of optical bandgap energy with CeO_2 content in $23B_2O_3$-5ZnO-$72Bi_2O_3$-x(CeO_2 in excess) glass.

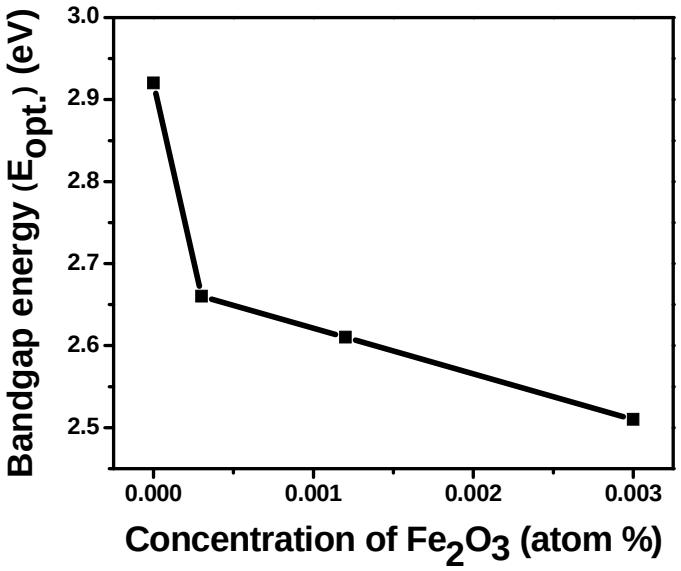

Fig. 6. Variation of optical bandgap energy with Fe_2O_3content in $23B_2O_3$-5ZnO-$72Bi_2O_3$-x(Fe_2O_3 in excess) glass.

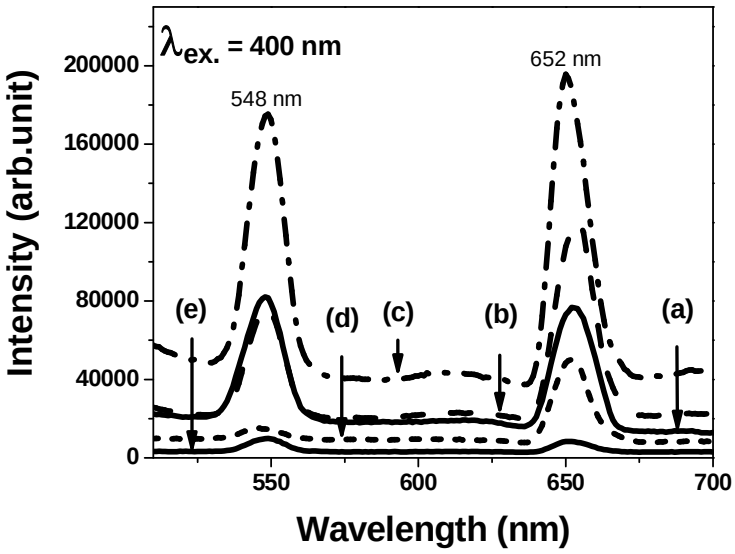

Fig. 7. Photoluminescence spectra of (a) 0 (base glass), (b) 0.0003, (c) 0.0012, (d) 0.003 and (e) 0.0058 atom % CeO_2 doped $23B_2O_3$-5ZnO-$72Bi_2O_3$ glasses at $\lambda_{ex.}$ = 400 nm.

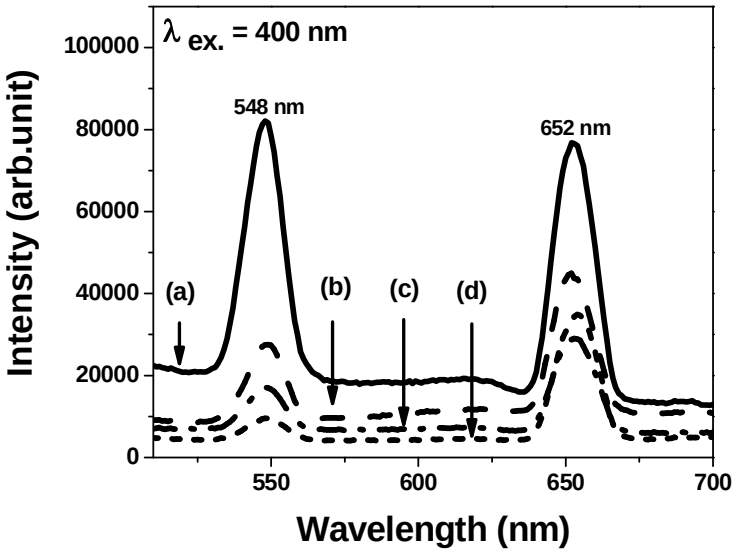

Fig. 8. Photoluminescence spectra of (a) 0 (base glass), (b) 0.0003 (c) 0.0012 and (d) 0.003 atom % Fe_2O_3 doped $23B_2O_3$-5ZnO-$72Bi_2O_3$ glasses at $\lambda_{ex.}$ = 400 nm.

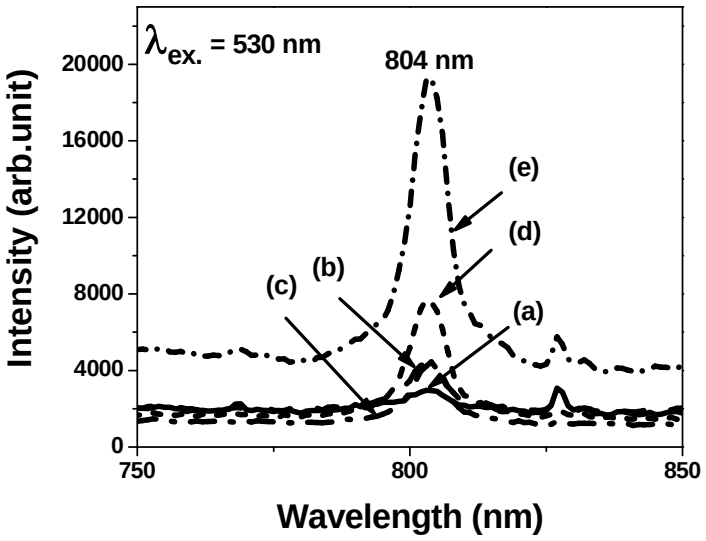

Fig. 9. Photoluminescence spectra of (a) 0 (base glass), (b) 0.0003, (c) 0.0012, (d) 0.003 and (e) 0.0058 atom % $CeO_{2\ doped\ 23B2}O_3$-5ZnO-72Bi_2O_3 glasses at $\lambda_{ex.}$ = 530 nm.

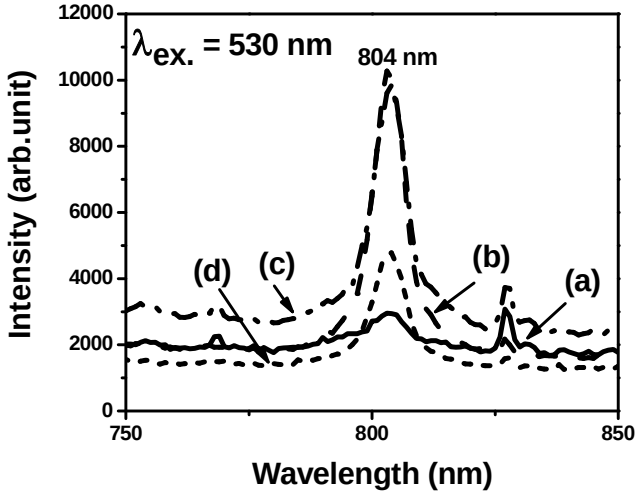

Fig. 10. Photoluminescence spectra of (a) 0 (base glass), (b) 0.0003 (c) 0.0012 and (d) 0.003 atom % Fe_2O_3 doped 23B_2O_3-5ZnO-72Bi_2O_3 glasses at $\lambda_{ex.}$ = 530 nm.